Catalytic Model Reactions for the HCN Isomerization. I. Theoretical Characterization of Some Water-Catalyzed Mechanisms

Fabrice Gardebien* and Alain Sevin

Laboratoire de Chimie Théorique, Université Paris VI,4, place Jussieu, case courrier 137, F-75252 Paris, France

Received: October 17, 2002; In Final Form: March 14, 2003

An ab initio study is presented for the HCN ⇌ HNC isomerization catalyzed by one, two, three, and four water molecules. Two mechanisms are proposed in the monohydrated case and one for each of the other cases. Four and six complexes have been determined on the mono- and the dihydrated potential energy surfaces, respectively, whereas only the reactant and product have been characterized for the tri- and tetrahydrated surfaces. For the monohydrated mechanisms, a reactant complex is connected to a product complex via the two determined saddle points, and these two complexes are separated by a reaction energy of 0.56 eV. A barrier lowering of 0.22 eV and a barrier increase of 0.17 eV are obtained compared to the monomolecular isomerization barrier T. For the dihydrated mechanism, the reaction energy between the reactant and product complexes is 0.55 eV, and this mechanism corresponds to a substantial barrier lowering of 0.95 eV compared to T. The corresponding further barrier lowerings for trihydration and tetrahydration are 0.58 and 0.42 eV, respectively. Reaction energy slightly decreases with the degree of hydration; the respective values are 0.51 and 0.48 eV. The existence of such hydrated isomerization pathways in water-dominated environments allows one to reconsider theoretical determination of the HNC/HCN ratio, for example, in the vicinity of icy surfaces.

I. Introduction

It is thought that comets could have played a role in the process of chemical evolution on earth, which finally led to life. Since events such as collisions or debris deposits could have triggered the chemical evolution on earth, the study of organic molecules detected on comets is of prime interest. The activity of comets arises as they approach the sun. Solar heating warms the comet nucleus, releasing gases and dust that form a spherical, diffuse cloud, the coma (whose visible part is extended up to 10^5 km around the nucleus), and the tails (dust and ion tails).

Various physicochemical processes occur because of interactions with solar wind and solar radiation in the outer parts of the coma whereas molecular collisions predominate in the inner coma. Because water ice is the main constituent of the nucleus, it is also the major volatile constituent. (Water comprised around 80% of the volatile of Comet Halley.) Hence, it is of interest to know the role played by vaporized water molecules in the reactivity of detected organic molecules. We are interested to know how the isomerization reaction for the detected HCN and HNC molecules[1,2] would be modified, provided that they are surrounded by water in the coma. This problem was also raised in a recent article by Irvine et al.[2] in *Nature*. There have been numerous studies on the monomolecular HCN ⇌ HNC isomerization reaction.[3−13] Possible formation mechanisms for species HCN and HNC were also proposed to account for the unrealistic abundance ratio HNC/HCN in interstellar clouds[14,15] (a ratio of 4.4 in the cold interstellar cloud L134).[16] We have found a recent publication dealing with the catalytic role of one water molecule during this isomerization,[17] and as far as we know, no previous investigation concerning the catalytic role of more water molecules exists. In the present work, we have considered several mechanisms with up to four catalytic water molecules. For monohydration, two mechanisms are presented whereas one mechanism is presented for each of the higher hydration cases. We have characterized these mechanisms by using quantum chemical calculations. For the sake of comparison, the stationary points of the potential energy surface (PES) of the isolated neutral isomerization have also been calculated.

The plan of this paper is as follows: After a description of the proposed mechanisms for reactions in section II, the computational methods that are used are presented in section III. Sections IV and V present the results of our proposed mechanisms for the monohydrated and dihydrated reactions, respectively, and the results for trihydration and tetrahydration are presented in section VI. Sections IV, V, and VI are each subdivided to allow us to discuss the geometric aspects of the respective stationary points and the energetic trends. A comparison between the monomolecular, monohydrated, and dihydrated pathways is also made at the end of the section V.

II. Description of the Isomerization Mechanisms

In this study, we consider mechanisms where a H_2O molecule interacts with HCN during the hydrogen migration process from carbon to nitrogen, thus playing a catalytic role in the reaction. Two mechanisms were considered: the first one merely corresponds to an interaction between the migrating hydrogen (from C to N) and the oxygen atom of the H_2O molecule (direct transfer mechanism); in the second one, the hydrogen atom bound to C migrates toward the oxygen atom while at the same time a hydrogen atom originally on the H_2O molecule is transferred toward nitrogen (indirect transfer mechanism). One can presume that in the latter mechanism the concomitant formation and rupture of the O···H bonds is concerted by virtue

* Corresponding author. E-mail: Fabrice.Gardebien@lct.jussieu.fr. Fax: ++32-65-37-33-66.

10.1021/jp022238a CCC: $25.00
Published on Web 04/23/2003

of energetic compensation resulting from the overall transfer process. We therefore tried to find a transition state where the two migrating hydrogens were at intermediate distance between C and O and O and N, respectively. Along the HCN + H_2O PES, we have characterized the two pathways corresponding to these two mechanisms that both proved to be concerted. In each pathway, one transition state was found: for the direct-transfer mechanism or pathway (a), the associated transition state will be hereafter noted T_a; for the indirect transfer or pathway (b), the transition state will be T_b. We have also characterized four complexes on this PES that were previously studied.[18−20] Heikkilä et al.[19] compared the experimentally determined frequencies for these complexes with the ab initio values they obtained with MP2/6-311++G(2d,2p) calculations. Two of the four complexes have a HCN·H_2O global formula and differ in their complexation site: the proton acceptor is either the oxygen, noted as H_2O···HCN or the (R) complex, or the nitrogen, noted as HCN···HOH or the (S) complex. The other two complexes of formula HNC·H_2O correspond to a hydrogen bond with O for the first one, noted as H_2O···HNC or the (P) complex, and with a C atom for the other, noted as HNC···HOH or the (Q) complex.

We also studied the isomerization reaction in the presence of two water molecules. The mechanism that was considered shares some similarities with the (b) path mechanism; the migration is concerted and occurs via a seven-membered-ring transition state labeled T_{2H}. The mechanism corresponds to three simultaneous hydrogen shifts: the hydrogen on carbon is transferred to the first water molecule, another hydrogen is transferred between the first and the second water molecules, and the latter transfers one hydrogen on the nitrogen end. As we will see, this reaction corresponds to an important barrier lowering and may thus apply to the case of the interstellar medium. One can suppose, although not unequivocally identified, the presence of HCN and HNC in the icy mantles of grains in the interstellar medium (since nitriles and isonitriles compounds have been detected).[21−23] Because water is the major ice constituent of grain mantles, upon UV heating of the grains HNC may isomerize according to this mechanism on account of both the barrier lowering and the interstellar cloud conditions (section V). A possible mechanism for DCN formation as well as for DNC disappearance in the concerned environments may be proposed. Six complexes have been determined on the dihydrated PES, three of which correspond to a HCN·$2H_2O$ global formula and the other three, to HNC·$2H_2O$. A systematic study of all complexes of this surface was not attempted.

Mechanisms similar to the preceding one were characterized for the trihydration and tetrahydration. The corresponding transition states are labeled T_{3H} and T_{4H}, respectively, and both have a cyclic structure allowing concerted transfers of protons in an analogous manner as for T_{2H}. The transition state T_{3H} is connected with a reactant, HCN·$3H_2O$, labeled A_{3H}, and with a product, HNC·$3H_2O$, labeled L_{3H}. The transition state T_{4H} is connected with a reactant and a product of global formulas, HCN·$4H_2O$, labeled A_{4H}, and HNC·$4H_2O$ labeled L_{4H}, respectively.

III. Methodology

All geometry optimizations were achieved using the Møller−Plesset second-order perturbation theory (MP2)[24] as implemented in the program system Gaussian 98.[25] The 6-311+G**[26−28] basis set was used during the geometry optimization to determine all minima and transition states of the neutral PESs. Single-point calculations were repeated on the stationary points with the coupled-cluster method with single, double, and noniterative inclusion of triple excitations (CCSD(T)[29,30]) using the same basis set. A correlated wave function is needed to account for the important correlation energy in these systems, mainly due to the multiple bond CN.[8,31] The reported energies are CCSD(T)/6-311+G** energies including zero-point energy (ZPE) and basis set superposition error (BSSE) corrections. The ZPE correction was calculated using the frequencies calculated at the MP2/6-311+G** level. The ZPE correction was calculated using the scaled harmonic vibrational frequencies. The appropriate scaling factors were taken from a study by Scott and Radom.[32] We used the counterpoise method of Boys and Bernardi[33] to correct for the BSSE. The MP2 method with a sufficiently large basis set has proved to be relevant for the optimization of neutral complexes.[34−37] The reported charges are taken from the Mulliken population analysis of the optimized structures. For the minima, we have verified that all eigenvalues of the respective Hessian matrix had positive values and that the Hessian matrix of each transition state had only one negative eigenvalue. When necessary, the connections between a transition state and the respective minima were confirmed by an intrinsic reaction coordinate (IRC) calculation,[38,39] which is defined as the steepest descent path on the PES starting from the transition-state geometry toward the reactant and product minima.

IV. Monohydrated Case

We have determined the minima connected to each transition state by following the intrinsic reaction coordinate (IRC). For both pathways, the reactant is complex (R), and the product, complex (P) displayed in Figure 1. Because complexes (S) and (Q) are not stationary points for any calculated pathways, their geometries will not be discussed. Thus, along the PES, the two paths associated with the two transition states T_a and T_b differ only for reaction coordinates lying between those of the reactant and product complexes. Both transition states are then connected via a second-order saddle point that corresponds to rearrangements of the H_3O entity in the vicinity of the CN bond; this stationary point will not be discussed further.

A. Geometries. 1. Complexes. Figure 1 displays the geometrical parameters of the four optimized complexes.

In each (R) and (P) complex, the H_2O molecule is a hydrogen bond acceptor. Both hydrogen bonds are linear, and both angles ∠O4···H3C and ∠O4···H5N are 179.7°. The linearity even extends for these complexes to the O, C, N, and H atoms (H of the H-bond). The symmetry of these complexes is pseudo-$C_{\infty v}$ with the distortion represented by the angle between the ON axis and the bisector of the water ∠HOH angle: the value of this angle is 23.6° for the H_2O···HCN complex and 29.7° for the H_2O···HNC complex. An experimental value of 20° was obtained for the former complex.[18] The r(O···H) distances are 2.065 and 1.808 Å in (R) and (P), respectively. The bond NH5 in (P) is stretched by 1.6%, and the elongation of the CH3 bond in (R) is half this value (0.8%). We can therefore suppose that the hydrogen bonding is stronger in (P) than in (R), as will be confirmed by the energy calculations. (See section IV.B.)

In Tables 1 and 2, the calculated frequencies for isolated molecules and complexes (R) and (P) are given. Experimental data are given for the sake of comparison. (See Tables for references.)

In the study by Heikkilä et al.[19] of the vibrational frequencies of the (R) complex, the experimental frequency shift for the CH stretching mode in the complex with respect to the HCN monomer value is −122 cm^{-1}. In this study, the corresponding

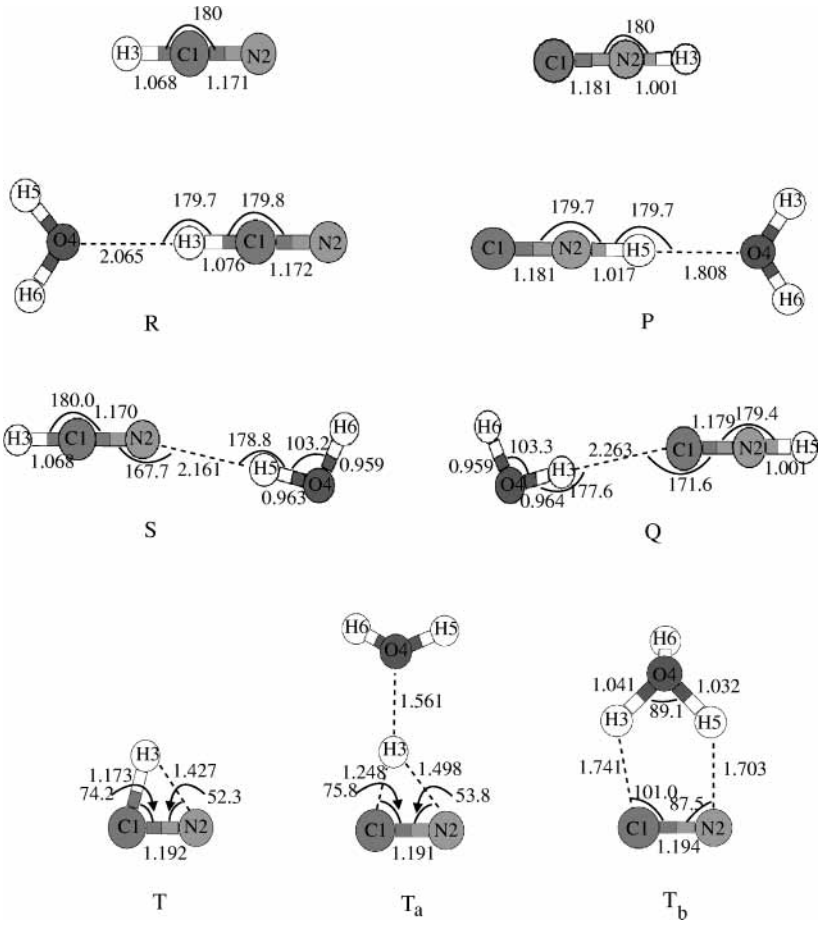

Figure 1. Geometries of the stationary points for the isolated isomerization (HCN, HNC mononers, and transition state T) and for the monohydrated isomerization reactions ((a) and (b) pathways) determined at the MP2/6-311+G** level. Bond lengths are in angstroms, and angles, in degrees.

TABLE 1: MP2/6-311+G Calculated and Experimental Frequencies (cm^{-1}) of the Separated and Complexed Reactants HCN + H_2O**

	HCN + H_2O		H_2O···HCN	
	exptl	calcd	exptl[a]	calcd
ν_{as}(OH)	3756[b]	3800.7	3740	3789.4
ν_s(OH)	3657[b]	3687.9	3635	3679.3
ν(CH)	3311[c]	3307.8	3182	3203.5
ν(CN)	2097[c]	2015.8[d]	2090	2013.0[d]
δ(HOH)	1595[b]	1546.7	1599	1559.7
δ(HCN) in plane	713[c]	693.0	827	853.3
δ(HCN) out of plane			815	819.6
ν intermol				266.5
ν intermol				184.7
ν intermol				140.7
ν intermol				118.0
ν intermol				108.0

[a] Reference 19. [b] Reference 53. [c] References 54 and 55. [d] Unscaled frequencies; see text.

TABLE 2: MP2/6-311+G Calculated and Experimental Frequencies (cm^{-1}) of the Separated and Complexed Products HNC + H_2O**

	HNC + H_2O		H_2O···HNC	
	exptl	calcd	exptl[a]	calcd
ν_{as}(OH)	3756[b]	3800.7		3786.2
ν_s(OH)	3657[b]	3687.9	3614	3677.4
ν(NH)	3653[c]	3642.3	3284	3352.7
ν(CN)	2029[c]	2014.9[d]	2031	2014.1[d]
δ(HOH)	1595[b]	1546.6		1562.2
δ(HNC) in plane	477[c]	486.8	819	855.3
δ(HNC) out of plane			731	773.0
ν intermol				305.7
ν intermol				240.8
ν intermol				186.6
ν intermol				127.9
ν intermol				117.8

[a] Reference 19. [b] Reference 53. [c] References 45, 56, and 57. [d] Unscaled frequencies; see text.

shift is -104 cm^{-1}. The experimental frequency shift for the NH stretching mode in (P) relative to that of the free HNC monomer is -336 cm^{-1}; we found a value of -290 cm^{-1}. As expected, the greatest red shift for the CH or NH elongation is observed for the complex having the strongest H-bond. The CN stretching frequencies for monomers HCN/HNC and their monohydrated complexes were unscaled because the calculated values are lower than the experimental ones. This is the consequence of the poor description of this electron-rich bond by the MP2 method based on the HF wave function (electron pairing around each nucleus leads to too much electron repulsion).[31,40−42] A higher level of geometry optimization and frequency calculations with the use of CCSD(T) gradient methods gives unscaled values of 2117 and 2047 cm^{-1} for monomers HCN and HNC, respectively.[6]

The C···O intermolecular distance was experimentally determined in the gas phase for complex (R).[18] The resulting experimental value of 3.152 Å is very close to our calculated value of 3.141 Å (0.3% error), indicating that the basis and the correlation method that were chosen are reliable for the characterization of such complexes.

2. T_a and T_b Transition States. The T_a transition state is characterized by an interaction between the water oxygen and the migrating hydrogen of HCN; its geometry is shown in Figure

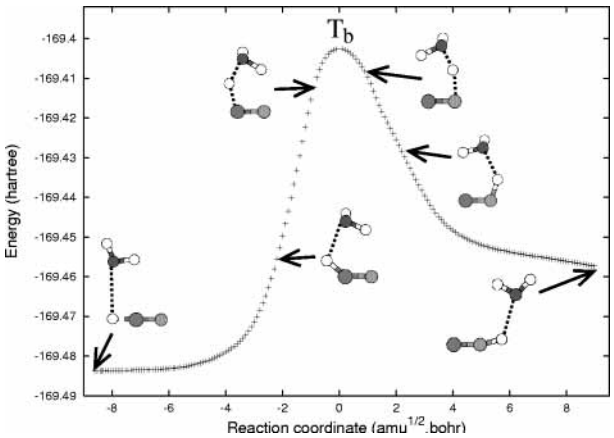

Figure 2. MP2/6-311+G** energy profile along reaction path (b). Only intermediate geometries between the transition state T_b and stationary points (R) and (P) are illustrated.

1. The reaction vector corresponds to H transfer between C and N atoms, and the associated frequency is 986.5i cm^{-1}. The angle between the O···H3 axis and the bisecting line of the ∠HOH angle (47.6°) indicates an orientation of the oxygen lone pair toward the migrating H. Furthermore, the *r*(O···H3) distance in the transition state is reduced by 0.504 Å compared to the corresponding distance in the (R) complex. All of these geometric features indicate a positive overlap between the atomic orbitals (AOs) centered both on the migrating H and on the oxygen atom.

The reduced *r*(O···H3) distance in the transition state that corresponds to an increasing orbital overlap between H and O atoms is favored by the electron deficiency on the migrating H atom, as shown by a partial positive charge of 0.40*e* on this hydrogen in the transition state. This positive charge results from the elongation of the CH bond. The charge on the CN fragment is −0.45*e*. The CH3 and NH3 bond distances, 1.248 and 1.498 Å, respectively, along with a ∠HCN value of 75.8° indicate a transition-state structure that is close to the reactants' structure though energetically close to the products HNC + H_2O (endothermic reaction).

The T_b transition state is characterized by a cyclic pentagonal structure, and its geometry is presented in Figure 1. In going from the reactant (R) complex to this transition state, the CH3 bond is broken, and the OH3 bond is formed. At the transition state, the distances *r*(OH5) = 1.032 Å, *r*(OH3) = 1.041 Å, *r*(NH5) = 1.703 Å, and *r*(CH3) = 1.741 Å clearly show two fragments interacting, and the transition state may be written as $[H3O\cdots CN]^{\ddagger}$. Furthermore, the charges are 0.74*e* on the H_3O moiety and −0.74*e* on CN, indicating that a proton (H3 in Figure 1) has been transferred from HCN to H_2O to form a transitory zwitterion species. As a result, the interaction between the two moieties is predominantly electrostatic in nature. The reaction vector consists of a rocking motion of the OH3 and OH5 bonds toward C and N atoms, the associated frequency being 643.5i cm^{-1}. The transfer of a second proton, H5, initially on a water molecule toward N leads to the product $H_2O\cdots HNC$ (Figure 2). Consequently, along path (b), a proton exchange between HCN and H_2O occurs. Similar values for *r*(OH3) and *r*(OH5) on one hand and for *r*(CH3) and *r*(NH5) on the other hand indicate a structure that is geometrically halfway between reactants and products although energetically closer to the separated products (endothermic reaction, see next section).

B. Energetic Aspect. The complexation energies between HCN and H_2O are 0.09 and 0.05 eV for the formation of $H_2O\cdots HCN$, (R), and $HCN\cdots HOH$, (S), respectively. The

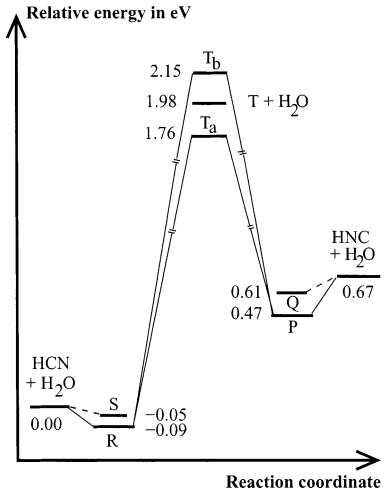

Figure 3. Reaction profile for the monohydrated reactions calculated at the CCSD(T)/6-311+G**//MP2/6-311+G** level and including both ZPE and BSSE corrections. The relative energies are defined with respect to HCN + H_2O in electronvolts.

complexation energies for $H_2O\cdots HNC$, (P), and $HNC\cdots HOH$, (Q), are 0.20 and 0.06 eV, respectively. The reactant and product complexes of the (a) and (b) pathways coincide with the thermodynamic complexes (R) and (P) of the PES. The reaction profiles for the monohydrated and isolated isomerization reactions are shown in Figure 3.

Recent determinations of the HCN/HNC energy difference as well as the barrier height for transition state T by Lee et al.[6] at a higher level of calculations gave values of 0.63 ± 0.04 eV and 1.93 ± 0.04 eV, respectively. The former quantity is consistent with experimental studies.[43,44] At our CCSD(T)/6-311+G**//MP2/6-311+G** level, the calculated HCN/HNC energy difference and T barrier height are both in good agreement with these previous studies (0.67 and 1.98 eV, respectively).

The monomolecular isomerization reaction is endothermic by 0.67 eV whereas the endothermicity of the monohydrated reaction (path (a) or (b)) is reduced to 0.47 or 0.56 eV when considering the complex $H_2O\cdots HNC$ to be the product of the reaction and HCN + H_2O or $H_2O\cdots HCN$ to be the reactant, respectively. The endothermicity is reduced because of the large complexation energy of $H_2O\cdots HNC$, which is about twice the corresponding energy for $H_2O\cdots HCN$. The resulting interaction with one water molecule therefore has an important effect on the relative stability of the reactant $H_2O\cdots HCN$ and the product $H_2O\cdots HNC$.

Starting from the (R) complex, there exists two distinct pathways leading to the same final (P) complex. The activated vibrational modes determine whether reaction occurs via T_a or T_b. When all modes are equally activated, the path with the smallest activation energy is the more likely. The transition state is placed at 1.98, 1.76, or 2.15 eV above the separated species HCN + H_2O for the monomolecular isomerization and for monohydrated paths (a) and (b), respectively. This comparison reveals that a large stabilization is brought by the interaction between one of the oxygen lone pairs and the migrating hydrogen along path (a).

Woon has published values of the activation energy relative to $H_2O\cdots HNC$ calculated at the MP2/6-31+G** + ZPE level and uncorrected for BSSE.[17] These values are 1.42 and 1.73 eV for paths (a) and (b), respectively. The author also obtained an activation energy for the reverse monomolecular reaction of 1.40 eV. Our corresponding CCSD(T)/6-311+G**//MP2/6-

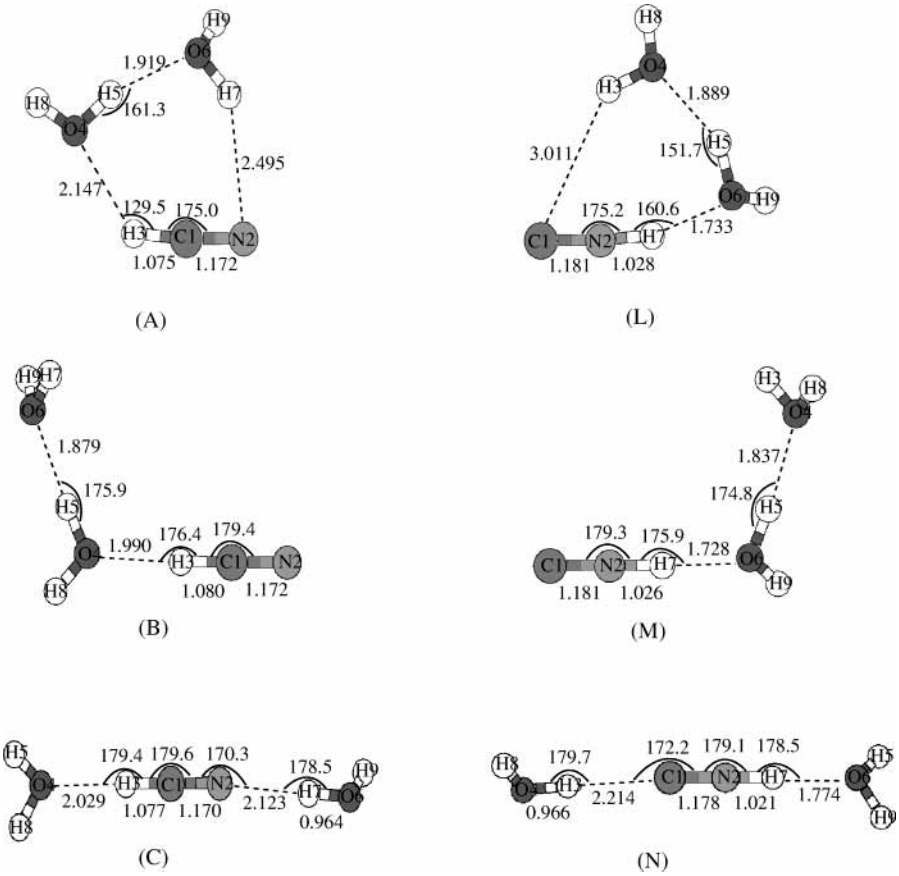

Figure 4. Equilibrium geometries of the dihydrated structures determined at the MP2/6-311+G** level. Bond lengths are in angstroms, and angles, in degrees.

311+G** + ZPE values, corrected for BSSE, are 1.29 and 1.68 eV for paths (a) and (b), respectively, and 1.31 eV for the monomolecular HNC isomerization.

In the absence of frequent molecular collisions (as it is the case in the lowest density region of the cometary comas), the energy gained upon the complexation of reactants HCN + H_2O cannot be released and is then distributed among the vibrational modes; thus, the energy to overcome the lowest barrier T_a is 1.76 eV. This energy is rather high, and at low temperature, the corresponding reaction is forbidden. However, when one considers the reaction at high temperature, some new equilibrium ratio values can be obtained.[2,45,46]

V. Dihydrated Case

In the monohydrated case, we have seen that the interaction with one H_2O molecule had strong consequences for the system: barrier lowering and a decrease in the reaction energy. In our study of the isomerization, we have introduced a second H_2O molecule to examine its effect on the reaction energetics. We have verified that in the transition-state geometry the direction of negative curvature corresponds to three asymmetric stretchings. We have established the connection between the transition state and the reactant complex labeled (A) and the product complex labeled (L) by an IRC calculation.

A. Geometries. 1. Complexes. The structures of the six complexes on which our discussion is based are displayed in Figure 4. In complexes (A) and (L), the HCN/HNC fragment acts as a proton donor to the $(H_2O)_2$ part. These complexes are also characterized by a long-range interaction between the more distant H_2O molecule and the CN part of the HCN/HNC fragment.

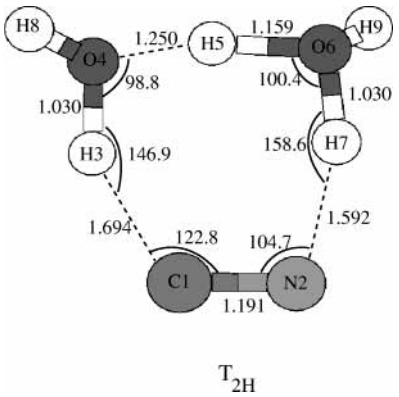

Figure 5. Transition-state geometry for the dihydrated reaction determined at the MP2/6-311+G** level. Bond lengths are in angstroms, and angles, in degrees.

In the (A) and (L) complexes, the latter secondary interaction leads to the formation of a cyclic structure. The atoms labeled 1−7 (Figure 4), being part of the cycle, are almost coplanar in both cases. (Dihedral angles ∠O6H7NC, ∠H7O6H5O4, and ∠H5O4H3C in (A) and ∠O4H3CN, ∠H3O4H5O6, and ∠H5O6H7N in (L) have values inferior to 9°.) It is worth comparing some relevant values of the geometric parameters in (A) and (R) of the preceding section: in (A), the ∠CH3···O4 angle decreases by 50.3°, the CH3 bond distance decreases by 0.001 Å, and the O4···H3 distance increases by 4%; the CH···O linkage is thus weakened. Conversely, the comparison between the parameters of the (P) complex and corresponding parameters in (L) shows a strengthening of the O···HN linkage for (L): distortion of the ∠NH7···O6 angle by 19.1°, lengthening of the NH7 bond by 1.1%, and shortening

TABLE 3: Scaled Frequencies (cm^{-1}) Calculated at the MP2/6-311+G Level for the Reactant (A) and the Product (L)**

		$HCN{\cdot}2H_2O$ (A)		
ν(OH)	3772.0	3766.9	3657.7	3553.5
ν(CH)	3228.1			
ν(CN)	2017.5[a]			
δ(HOH)	1584.3	1571.5		
ν	781.6	738.4	653.3	435.3
	327.8	251.8	201.9	186.8
	170.0	146.1	105.1	99.5
	58.3			
		$HNC{\cdot}2H_2O$ (L)		
ν(OH)	3775.5	3757.6	3662.7	3540.8
ν(NH)	3170.6			
ν(CN)	2003.2[a]			
δ(HOH)	1570.8	1565.9		
ν	929.8	857.0	642.3	395.4
	326.3	267.4	238.5	219.8
	198.7	144.9	136.4	122.8
	53.8			

[a] Unscaled frequencies; see section IV A.

of the O6···H7 bond by 4%. The ∠O···HC value in (A) is smaller by 31.1° than the ∠O···HN value in (L), which brings the more distant H_2O molecule closer to the CN bond in complex (A). Thus, we see that in complex (A) the O ··· HC linkage is weakened compared to that in (R) in favor of a long-range interaction that is stronger than the corresponding interaction in (L).

In (A), it is noteworthy that *r*(N···H7) is only 16% longer than *r*(O4···H3) (in (L), *r*(C···H3) is 74% longer than r(O6···H7)), indicating strong H-bond character for the N···H7 linkage. The effects of the long-range interaction in the (A) and (L) complexes can be seen in the deviation of about 5° for the ∠HCN and ∠HNC angles, respectively. This indicates a perturbation of the π_{CN} bond by the more distant water molecule and thus that part of this interaction corresponds to an overlap between orbitals of the concerned fragments. The determination of other complexes (B) and (M) (Figure 4) with the same H-bonds as in (A) and (L) but with no long-range interaction indeed shows little deviation from the straight angle for ∠HCN and ∠HNC (179.4° and 179.3°, respectively). The scaled vibrational frequencies calculated for (A) and (L) are reported in Table 3.

In complexes (B) and (M) (open structures), all H-bond angles differ by less than 5° from linearity. Going from (A) to (B) corresponds to shortening the O4···H3 and O6···H5 linkages by 0.157 and 0.040 Å, respectively, and to increasing the *r*(CH3) distance by 0.005 Å. These geometry perturbations reveal a strengthening of both H-bonds upon changing from (A) to (B). The same conclusion is less striking when going from (L) to (M): O4···H5 and O6···H7 bond distances decrease by 1 order of magnitude less (0.052 and 0.005 Å), and *r*(NH7) even decreases by 0.002 Å.

Each of the last two determined complexes (C) and (N) has one H-bond with one H_2O molecule as an acceptor of the HCN/HNC hydrogen and another one with a second H_2O molecule as a donor to the nitrogen of HCN or to the carbon of HNC. We will not discuss the geometries of (C) and (N), presented in Figure 4, because (C) is less stable than (A) and (B) and complex (N) is less stable than (L) and (M). (See section V.B.) Despite a careful search, we found no dihydrated complexes corresponding to nitrogen in HCN or carbon in HNC, as a proton acceptor of one H_2O molecule, a H-bond linkage already existing between the two H_2O molecules. All optimization attempts converged to previously obtained complex (A) or (L) by the translation of the $HOH{\cdots}OH_2$ entity along the HCN or HNC axis.

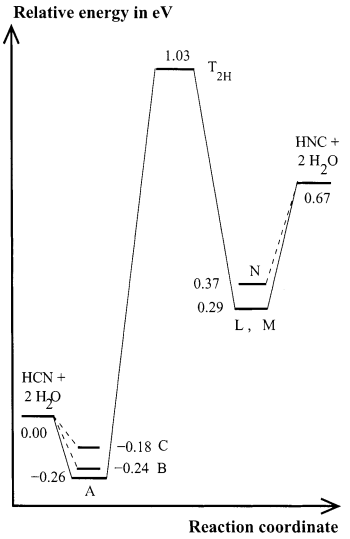

Figure 6. Reaction profile for the dihydrated reaction calculated at the CCSD(T)/6-311+G**//MP2/6-311+G** level and including both ZPE and BSSE corrections. The relative energies are defined with respect to HCN + 2 H_2O in electronvolts.

2. Transition State. The geometry of the transition state T_{2H} is an almost planar cyclic structure (with the exception of H8 and H9) and is presented in Figure 5.

This structure corresponds to an interaction between two fragments H_5O_2 and CN (*r*(O4H3) = *r*(O6H7) = 1.030 Å, *r*(NH7) = 1.592 Å, *r*(CH3) = 1.694 Å); the former moiety is similar to the proton-transfer transition-state geometry in the case of the protonated water dimer. The charges displayed on these fragments are 0.76*e* on H_5O_2 and −0.76*e* on CN, revealing an ionic pair interaction for this transition state. The simultaneous motions of the three in-plane hydrogens have been identified as the reaction vector (C···H3−O4, O4···H5···O6, and O6−H7···N stretchings). It appears that the transition-state structure T_{2H} is similar to structure T_b with a second H_2O molecule taking part in the cyclic arrangement.

The OH bond distances for out-of-plane hydrogens H8 and H9 are only slightly perturbed by the in-plane migrations (increase by ∼0.005 Å for these two OH bonds). The CN elongation (increases of 1.6% and 0.8% relative to (A) and (L), respectively) is consistent with a developing negative charge on the CN moiety because the CN bond lengths decrease in the order CN^- > HNC > HCN.[34] The differences between C···H3 and N···H7 distances on one hand and of O4···H5 and O6···H5 distances on the other hand indicate a late character in agreement with the reaction endothermicity.

B. Energetic Aspect. In Figure 6, the stationary points of the PES are presented. Complexes (C) and (N) are not favored thermodynamically; they are both less stable by 0.08 eV than the more stable complexes (A) and (L). This is related to the H_2O dimer bonding energy that provides a greater stabilization for (A) and (B) relative to (C) and for (L) and (M) relative to (N).

Complexes (M) and (L) are isoenergetic at our level of calculation. The additional interaction in (L), compared to that in (M), has no stabilization effect whereas it is responsible for the stabilization of (A) relative to (B), even with two stronger H-bonds (CH3···O4 and O4H5···O6) in the latter complex. The greater stabilization of (A) is due to the N···H7 interaction, which can be considered to be a third weak H-bond. In any

cases, we can assume that the barrier connecting the cyclic and open structures is very low. Its presence is caused by the weak interaction N···H7 (or C···H3), which upon cancellation induces a small energy variation along the path between (A) and (B) (or (L) and (M), respectively).

The activation energy from the separated species HCN + 2 H_2O is 1.03 eV; a substantial lowering of 0.95 eV is obtained relative to the activation energy of the monomolecular case. The activation energy from HNC + 2 H_2O is 0.36 eV. The reverse reaction can account for isotopic exchange between DNC and H_2O in the cometary coma where the low-density conditions limit complexation energy removal due to collisions with neighboring molecules. The reverse reaction also supposes that reactants HNC (or DNC) + 2 H_2O had an excess energy of 0.36 eV either as internal energy or kinetic energy.

$$DNC + 2\ H_2O \rightleftharpoons HCN + H_2O + HDO$$

In addition, since the HDO/H_2O ratio in Comet Halley is about twice the terrestrial value, another possible deuterium transfer is

$$HNC + HDO + H_2O \rightleftharpoons DCN + 2\ H_2O$$

In circumstellar environments, HCN and HNC molecules are presumably trapped in icy mantles (mainly composed of water ice) of grains. Upon UV heating, excess internal energy for HNC (or DNC) of 0.36 eV along with a low collisional probability for the formed hydrated complexes may account for isotopic exchange according to this mechanism.

C. Comparison of the Different Pathways. Along the pathway between the isolated HCN reactant and the transition state T in the monomolecular process, the geometrical parameters responsible for energy change are the ∠HCN bending angle and the CN and CH stretchings. A previous study[3] has shown that the *r*(CN) parameter varied only slightly along the path (maximum amplitude of ∼0.05 Å; for HCN in equilibrium geometry, such a CN elongation raises its energy by 0.1 eV). Because CN bond-length variation remains small along the path, the resulting contribution to the destabilization energy (activation energy) is therefore expected to be negligible. We will then consider that all geometrical features minimizing the destabilization due to ∠HCN variation or CH stretching lower the barrier height of the isomerization. We will see then that T_a and T_{2H} have some of these characteristics.

Geometries of T and T_a are reported in Figure 1. For the T_a transition state, the HCN triangle appears as if one had stretched the hydrogen side, increasing the *r*(CH) parameter by 6% and *r*(NH) parameter by 5%, leaving *r*(CN) almost unperturbed; the ∠HCN and ∠HNC angles are increased by only 1° compared to the corresponding values in T (Figure 1). Thus, the stretching on the hydrogen side corresponds to the removal of the migrating H away from the CN fragment, and this feature has two consequences. First, the interaction between the 1s AO of H and the π and π^* MOs of the CN part decreases. The second consequence is an increase in both positive charge on H (+0.15*e*) and negative charge on CN (−0.1*e* on each of the C and N atoms) with respect to the charge on these three atoms in the monomolecular T transition state. The first of these two consequences corresponds to a reduction of the orbital overlap, and the second one implies an increase of the electrostatic interactions between the fragments H and CN; these features have also been previously noted by Rao et al.[13] for the LiCN/LiNC isomerization. Along the path between the reactant complex and the T_a transition state, the charges on H and CN increase because of the polarization of the CH bond; the ∠HCN bending becomes easier owing to isotropic electrostatic forces that become more important. The other stabilizing feature of the T_a transition state corresponds to the stabilization due to the important orbital overlap between the migrating H and the H_2O molecule trying to compensate for the destabilization induced by the CH stretching. In summary, in T_a, the ∠HCN bending is facilitated by electrostatic forces, and the CH stretching is compensated by a positive orbital overlap.

For both pathways from respective reactant to the T_b or T_{2H} transition state, a proton is transferred between HCN and the H_2O or $(H_2O)_2$ entity, respectively. Both transition states T_b and T_{2H} are characterized by an ionic pair interaction whereas a covalent interaction predominates along the path in the monomolecular case.

The ∠HCN value in transition structure T_{2H} is larger by 21.8° than the corresponding value in T_b and by 48.6° than the value in T; the ∠HNC value in T_{2H} is also larger by 17.2° and by 52.4° compared to the values in T_b and T, respectively. The C···H3 distance is almost the same for structures T_{2H} and T_b (1.694 and 1.741 Å, respectively), and N···H7 is inferior by 6% to the N···H5 distance. The CN distance is also almost identical for the latter two structures. Then, besides the difference for angle deformation ∠HCN/∠HNC in transition states T_b and T_{2H}, the main difference is related to the H_3O^+ and $H_5O_2^+$ moieties in the respective structures and particularly to the different proton affinities associated with the water molecule and its dimer. The difference between the activation energy for the monohydrated path (b) and the dihydrated path (relative to respective separated species) is 1.12 eV, which represents 76% of the calculated proton affinity difference of H_2O and $(H_2O)_2$, 1.48 eV. Thus, the large proton affinity of the water dimer compensates for the destabilization due to CH stretching and explains, along with the lesser ∠HCN angle deformation (compared to T or T_b), the stabilization of the T_{2H} barrier relative to separated reactants.

Whereas transition states T and T_a have an early character, T_b is halfway between the separated reactants and products, and T_{2H} has a late character consistent with the energetic proximity of T_{2H} and the separated products.

VI. Higher Degree of Hydration

The isomerization was further studied with the participation of three and four water molecules. On the respective potential energy surfaces, a reactant complex, A_{3H} or A_{4H}, and a product, L_{3H} or L_{4H}, are connected to a transition state, T_{3H} or T_{4H}. The corresponding geometries are displayed in Figures 7 and 8. For the transition states, we have ensured that the eigenvector associated with the negative eigenvalue of the respective Hessian corresponds to the transfer of a hydrogen between atoms C and N. Scaled vibrational frequencies are reported in Tables 4 and 5 for the equilibrium geometries. Reaction profiles are presented in Figure 9 and will be discussed in section VI.B.

A. Geometries. 1. Complexes. For each of the complexes A_{3H}, L_{3H}, A_{4H}, and L_{4H}, a cyclic structure is observed that results from the interaction of HCN or HNC with a chainlike water cluster. The distances N···H9 and N···H11 in A_{3H} and A_{4H} are 2.124 and 1.988 Å, respectively. The analogous bonds C···H3 in L_{3H} and L_{4H} have distances of 2.360 and 2.049 Å, respectively. An almost planar structure is obtained for complexes A_{3H} and L_{3H}, and the dihedral angles for the atoms labeled from 1 to 9 are less than 15°. The dihedral angles for atoms labeled from 1 to 11 in A_{4H} and L_{4H} are less than 35°.

2. Transition States T_{3H} and T_{4H}. The structure obtained for T_{3H} consists of four interacting fragments H_3O, CN, and

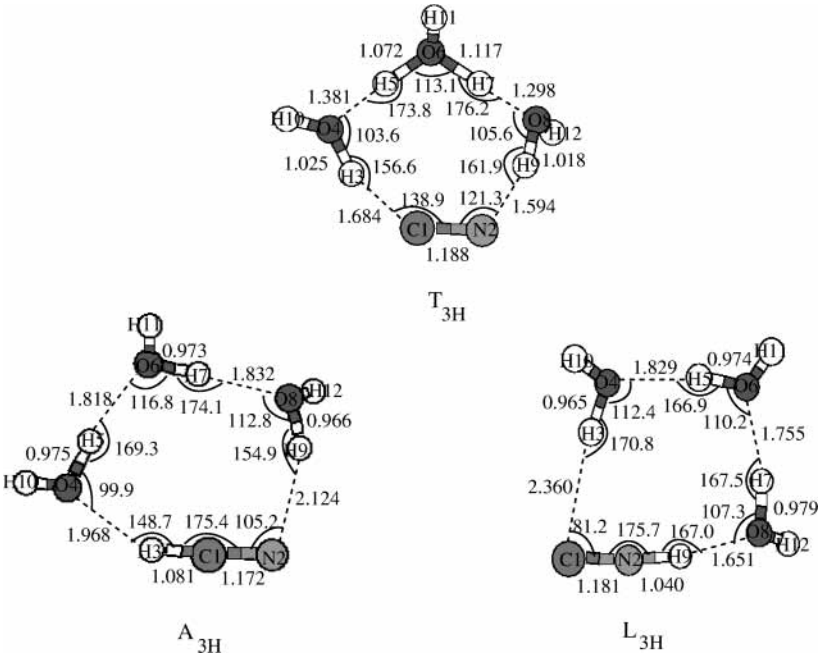

Figure 7. Geometries of the stationary points for the trihydrated pathway (reactant A_{3H}, transition state T_{3H}, and product L_{3H}) determined at the MP2/6-311+G** level. Bond lengths are in angstroms, and angles, in degrees.

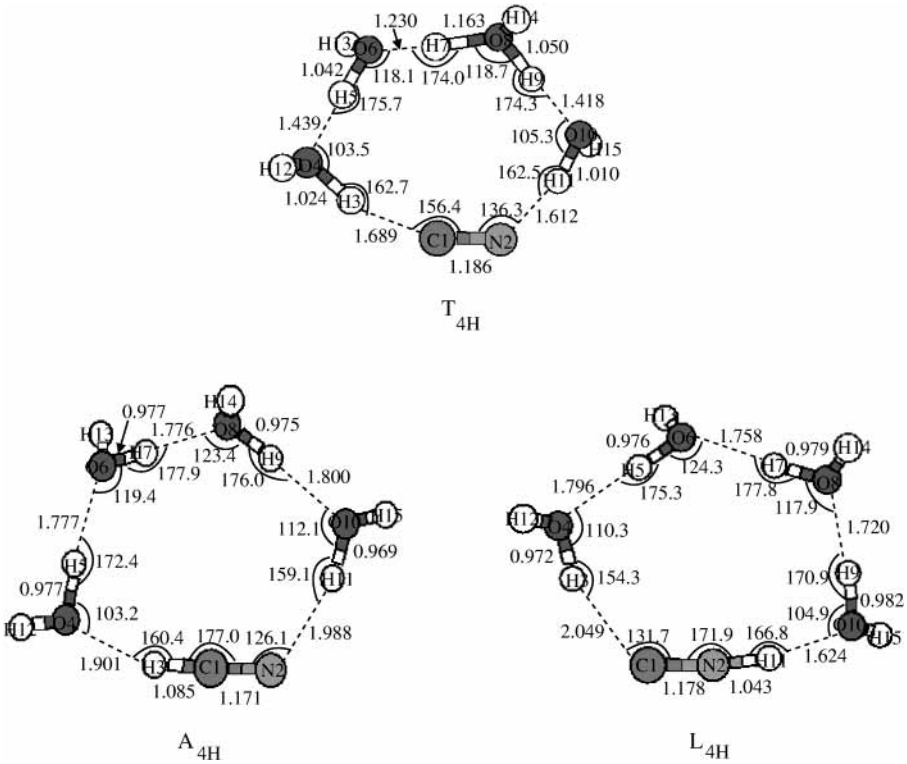

Figure 8. Geometries of the stationary points for the tetrahydrated pathway (reactant A_{4H}, transition state T_{4H}, and product L_{4H}) determined at the MP2/6-311+G** level. Bond lengths are in angstroms, and angles, in degrees.

two H_2O monomers. For the H_3O fragment, the calculated charge is 0.75*e*, and the distances *r*(O6H5) and *r*(O6H7) are 1.072 and 1.117 Å, respectively. The calculated negative charge, −0.80*e*, is shared by atoms C and N.

In T_{4H}, a bridged structure O···H···O exists as observed in T_{2H}. The two associated distances *r*(O···H) in T_{4H} are 1.163 and 1.230 Å, and the corresponding values in T_{2H} are 1.159 and 1.250 Å. The geometry of T_{4H} consists of four interacting fragments CN^- (with a calculated charge of −0.83*e*), $H_5O_2^+$ (0.76*e*), and two water molecules.

An almost planar structure is observed for the atoms of the cycle of T_{3H} labeled from 1 to 9; the associated dihedral angles are inferior to 20°. For T_{4H}, the atoms labeled from 1 to 11 are almost coplanar; the associated dihedral angles are less than 35° except for ∠H5O6O8H9, whose value is 48°.

B. Energetic Aspect. The reaction profiles for the dihydrated, trihydrated, and tetrahydrated paths are represented in Figure 9. The reaction energy does not vary with the degree of hydration: 0.51 and 0.48 eV for the trihydrated and tetrahydrated paths, respectively. Starting from the respective reactant

TABLE 4: Scaled Frequencies (cm^{-1}) Calculated at the MP2/6-311+G Level for the Reactant A_{3H} and the Product L_{3H}**

			HCN·3H$_2$O (A_{3H})			
ν(OH)	3762.3	3761.9	3752.7	3617.9	3495.0	3444.2
ν(CH)	3130.5					
ν(CN)	2015.4[a]					
δ(HOH)	1616.3	1591.5	1575.4			
ν	854.2	829.4	781.3	727.9	481.3	431.1
	387.8	300.9	253.1	233.7	212.8	193.9
	178.8	168.0	139.9	130.0	117.8	51.0
	40.1					
			HNC·3H$_2$O (L_{3H})			
ν(OH)	3759.9	3757.9	3749.7	3626.5	3488.8	3387.6
ν(CH)	2990.4					
ν(CN)	1997.4[a]					
δ(HOH)	1619.9	1593.8	1580.1			
ν	1022.5	935.4	782.2	649.5	486.3	452.0
	395.2	301.7	293.9	255.8	232.0	188.5
	181.2	148.9	147.9	126.0	104.6	63.4
	32.3					

[a] Unscaled frequencies; see section IV A.

TABLE 5: Scaled Frequencies (cm^{-1}) Calculated at the MP2/6-311+G Level for the Reactant A_{4H} and the Product L_{4H}**

				HCN·4H$_2$O (A_{4H})				
ν(OH)	3758.8	3757.0	3754.6	3752.9	3567.6	3464.8	3437.6	3384.5
ν(CH)	3069.5							
ν(CN)	2017.6[a]							
δ(HOH)	1628.3	1607.4	1593.6	1579.4				
ν	900.0	876.2	841.7	784.4	752.9	548.7	444.7	434.0
	397.5	336.6	271.3	265.8	235.8	233.9	207.9	199.9
	173.4	172.1	152.6	143.5	140.0	56.3	43.9	38.0
	31.6							
				HNC·4H$_2$O (L_{4H})				
ν(OH)	3752.5	3751.4	3750.2	3749.3	3503.1	3438.4	3383.5	3307.5
ν(CH)	2925.5							
ν(CN)	2012.1[a]							
δ(HOH)	1632.1	1610.0	1593.2	1579.1				
ν	1054.1	968.0	869.2	819.6	772.9	585.7	480.7	451.0
	413.6	356.5	318.3	289.8	265.1	259.8	232.8	219.3
	187.2	178.9	164.0	158.0	141.5	62.6	49.4	43.6
	38.3							

[a] Unscaled frequencies; see section IV A.

complex, the required energies to overcome the barriers T_{2H}, T_{3H}, and T_{4H} are 1.29, 1.00, and 0.83 eV. Thus, we can see that the monomolecular isomerization barrier of 1.98 eV is lowered by 0.69 eV with dihydration whereas trihydration and tetrahydration bring further lowerings of only 0.29 and 0.17 eV, respectively. The activation energies for the isomerization of HNC from the complexes L, L_{3H} and L_{4H} are 0.74, 0.49, and 0.35 eV, respectively.

The reactivity in the gas phase starting from separated reactants HCN or HNC + 3 or 4 H_2O is unlikely. Yet, in the immediate vicinity of icy sublimating surfaces (mainly composed of H_2O ice) where molecular densities are highest, interactions between two preliminarily formed hydrated complexes are likely. For interactions between hydrated HCN or HNC and a small water cluster, the conversion of nondissipated complexation energy in the modes leading to geometry T_{3H} or T_{4H} may occur, thus providing a mechanism for isomerization. Table 6 presents the relative energies for the following systems HCN/HNC·$(H_2O)_{a-n}$ + $(H_2O)_n$ with $a = \{3; 4\}$ and $1 \leq n \leq a$. $(H_2O)_n$ refers to the most stable complex resulting from the interaction of n water molecules. (Cyclic structures are obtained for the trimer and tetramer; see, for example, ref 47.) The relative energies for the systems HCN·$(H_2O)_{a-n}$ + $(H_2O)_n$ with $a = \{3; 4\}$ indicate that isomerization of HCN cannot occur via barriers T_{3H} or T_{4H}.

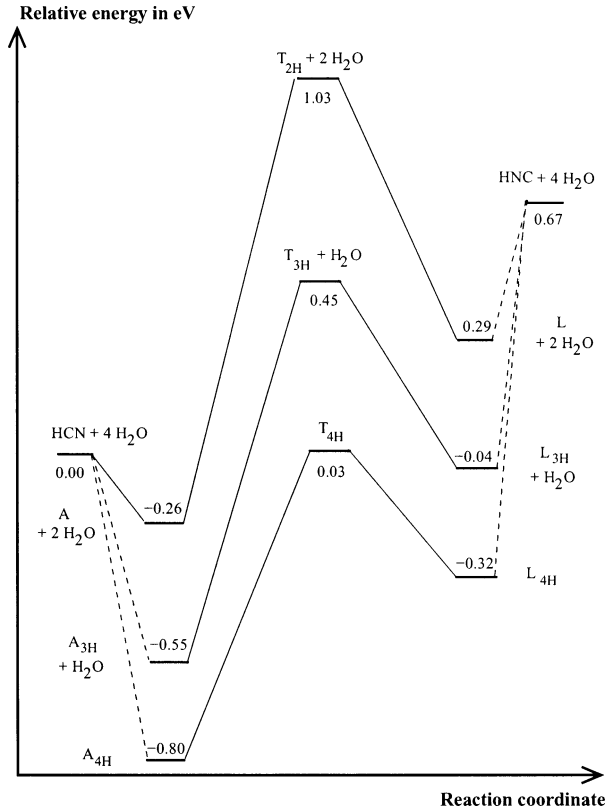

Figure 9. Reaction profiles for the dihydrated, trihydrated, and tetrahydrated pathways calculated at the CCSD(T)/6-311+G**//MP2/6-311+G** level and including both ZPE and BSSE corrections. The relative energies are defined with respect to HCN + 4 H_2O in electronvolts.

TABLE 6: Relative Energies for the Systems HCN·$(H_2O)_{3-n}$ + $(H_2O)_n$, HNC·$(H_2O)_{3-n}$ + $(H_2O)_n$ (n = 1,...3), HCN·$(H_2O)_{4-m}$ + $(H_2O)_m$, and HNC ·$(H_2O)_{4-m}$ + $(H_2O)_m$ (m = 1,...4) Calculated at the CCSD(T)/6-311+G//MP2/6-311+G** Level and Corrected for Both ZPE and BSSE**

HCN·$(H_2O)_{3-n}$ + $(H_2O)_n$		HNC·$(H_2O)_{3-n}$ + $(H_2O)_n$	
species	E_{rel}	species	E_{rel}
HCN + 3 H_2O	0.00	HNC + 3 H_2O	0.67
HCN + $(H_2O)_3$	−0.33	HNC + $(H_2O)_3$	0.33
R + $(H_2O)_2$	−0.18	P + $(H_2O)_2$	0.38
A + H_2O	−0.26	L + H_2O	0.29
HCN·$(H_2O)_{4-m}$ + $(H_2O)_m$		HNC·$(H_2O)_{4-m}$ + $(H_2O)_m$	
species	E_{rel}	species	E_{rel}
HCN + 4 H_2O	0.00	HNC + 4 H_2O	0.67
HCN + $(H_2O)_4$	−0.62	HNC + $(H_2O)_4$	0.05
R + $(H_2O)_3$	−0.42	P + $(H_2O)_3$	0.14
A + $(H_2O)_2$	−0.34	L + $(H_2O)_2$	0.21
A_{3H} + H_2O	−0.55	L_{3H} + H_2O	−0.04

The relative energies for the systems HNC·$(H_2O)_{3-n}$ + $(H_2O)_n$ (n = 1,...3) are 0.33, 0.38, and 0.29 eV for HNC + $(H_2O)_3$, P + $(H_2O)_2$, and L + H_2O, respectively. Thus, reverse isomerization may occur via T_{3H} only if an excess energy of 0.12, 0.07, or 0.16 eV is available, respectively. The isomerization of HNC has a greater probability of occurring from the interaction of P and a water dimer owing to the smaller excess energy required in this case. The systems HNC·$(H_2O)_{4-n}$ + $(H_2O)_n$ (n = 1,...4) have relative energies of 0.05, 0.14, 0.21, and −0.04 eV for HNC + $(H_2O)_4$, P + $(H_2O)_3$, L + $(H_2O)_2$, and L_{3H} + H_2O, respectively. The isomerization of HNC may result from all of the preceding interactions if one supposes an intramolecular redistribution of the accumulated complexation energy for the respective system.

In regions surrounding a star or a protostar where temperatures can be as high as several hundred Kelvin, the icy mantles of grains mainly composed of H_2O[48] are sublimated. The above-discussed mechanisms may thus apply in the near vicinity of these grains where one can suppose the formation of such complexes when HNC is initially present frozen onto the grain mantles.

Experimental studies are in progress using rare gas matrixes technique[49] to investigate the presented isomerization pathways for HNC.

VII. Conclusions

We have studied some water-catalyzed pathways for the HCN isomerization. For the monohydrated paths, four stable complexes have been characterized, and the more stable reactant complex and product complex are connected via two saddle points T_a and T_b (1.76 and 2.15 eV with respect to HCN + H_2O), which are, respectively, stabilized by 0.22 eV and destabilized by 0.17 eV with respect to the monomolecular isomerization barrier T (1.98 eV). The reaction energy between the reactant and product complexes is 0.56 eV.

On the dihydrated PES, six complexes as well as a saddle point T_{2H} connecting the most stable determined reactant and product complexes have been characterized. The reaction energy separating the most stable reactant and product is about the same as for the complexes in the monohydrated case, 0.55 eV, and the barrier is 1.03 eV above the separated reactant HCN + 2 H_2O. Despite a lowering of the barriers under a water catalytic effect, the HCN isomerization remains difficult for the mono- and dihydrated pathways.

Mechanisms considering trihydration and tetrahydration were also characterized. The reaction energies are 0.51 and 0.48 eV, respectively. The isomerization of HCN is not likely to occur; however, interactions on icy grain surfaces either between the complexes $HNC\cdot(H_2O)_{4-n}$ and $(H_2O)_n$ (for $n = 1, 2, 3, 4$) or between the more stable structure for $HNC\cdot H_2O$ and a water dimer can account for the observed decrease of the ratio HNC/HCN in some regions of some giant molecular clouds such as the Orion Molecular Cloud.[50,51,52] Further experiments are needed to provide data related to the proportion and lifetime of the hydrated HNC species formed in the gas phase as they sublimate from HNC-containing ice mixtures.

References and Notes

(1) Krishna Swamy, K. S. *Physics of Comets*; World Scientific Publishing Company Singapore, 1986.

(2) Irvine, W. M.; Morvan, D. B.; Lis, D. C.; Matthews, H. E.; Biver, N.; Crovisier, J.; Davies, J. K.; Dent, W. R. F.; Gautier, D.; Godfrey, P.D.; Keene, J.; Lovell, A. J.; Owen, T. C.; Phillips, T. G.; Rauer, H.; Schloerb, F. P.; Senay, M.; Young, K. *Nature (London)* **1996**, *383*, 418.

(3) Pearson, P. K.; Schaefer, H. F., III; Wahlgren, U. *J. Chem. Phys*. **1975**, *62*, 350.

(4) Bowman, J. M.; Gazdy, B.; Bentley, J. A.; Lee, T. J.; Dateo, C. E. *J. Chem. Phys*. **1993**, *99*, 308.

(5) Gazdy, B.; Musaev, D. G.; Bowman, J. M.; Morokuma, K. *Chem. Phys. Lett*. **1995**, *237*, 27.

(6) Lee, T. J.; Rendell, A. P. *Chem. Phys. Lett*. **1991**, *177*, 491.

(7) Ishida, K.; Morokuma, K.; Komornicki, A. *J. Chem. Phys*. **1977**, *66*, 2153.

(8) Redmon, L. T.; Purvis, G. D., III; Bartlett, R. J. *J. Chem. Phys*. **1980**, *72*, 986.

(9) Bentley, J. A.; Bowman, J. M.; Gazdy, B.; Lee, T. J.; Dateo, C. E. *Chem. Phys. Lett*. **1992**, *198*, 563.

(10) Peric, M.; Mladenovic, M.; Peyerimhoff, S. D.; Buenker, R. J. *Chem. Phys*. **1984**, *86*, 85.

(11) Kumeda, Y.; Minami, Y.; Takano, K.; Taketsugu, T.; Hirano, T. *J. Mol. Struct.: THEOCHEM* **1999**, *458*, 285.

(12) Bowman, J. M.; Gazdy, B. *J. Phys. Chem. A* **1997**, *101*, 6384.

(13) Rao, V. S.; Vijay, A.; Chandra, A. K. *Can. J. Chem.* **1996**, *74*, 1072.

(14) Allen, T. L.; Goddard, J. D.; Schaefer, H. F., III. *J. Chem. Phys*. **1980**, *73*, 3255.

(15) Shiba, Y.; Hirano, T.; Nagashima, U.; Ishii, K. *J. Chem. Phys*. **1998**, *108*, 698.

(16) Wootten, A.; Evans, N. J., II; Snell, R.; Bout, P. V. *Astrophys. J*. **1978**, *225*, L143.

(17) Woon, D. E. *Icarus* **2001**, *149*, 277.

(18) Gutowsky, H. S.; Germann, T. C.; Augspurger, J. D.; Dykstra, C. E. *J. Chem. Phys*. **1992**, *96*, 5808.

(19) Heikkilä, A.; Pettersson, M.; Lundell, J.; Khriachtchev, L.; Räsänen, M. *J. Phys. Chem. A* **1999**, *103*, 2945.

(20) Rivelino, R.; Canuto, S. *Chem. Phys. Lett*. **2000**, *322*, 207.

(21) Bernstein, M. P.; Sandford, S. A.; Allamandola, L. J.; Chang, S. *Astrophys. J*. **1995**, *454*, 327.

(22) Whittet, D. C. B.; Schutte, W. A.; Tielens, A. G. G. M.; Boogert, A. C. A.; de Graauw, T.; Ehrenfreund, P.; Gerakines, P. A.; Helmich, F. P.; Prusti, T.; van Dishoeck, E. F. *Astron. Astrophys*. **1996**, *315*, L357.

(23) Sandford, S. A. *Astron. Inf. Spectrosc*. **1993**, *41*, 181.

(24) Moller, C.; Plesset, M. S. *Phys. Rev*. **1934**, *46*, 618.

(25) Frisch, M. J.; Trucks, G. W.; Schlegel, H. B.; Scuseria, G. E.; Robb, M. A.; Cheeseman, J. R.; Zakrzewski, V. G.; Montgomery, J. A., Jr.; Stratmann, R. E.; Burant, J. C.; Dapprich, S.; Millam, J. M.; Daniels, A. D.; Kudin, K. N.; Strain, M. C.; Farkas, O.; Tomasi, J.; Barone, V.; Cossi, M.; Cammi, R.; Mennucci, B.; Pomelli, C.; Adamo, C.; Clifford, S.; Ochterski, J.; Petersson, G. A.; Ayala, P. Y.; Cui, Q.; Morokuma, K.; Malick, D. K.; Rabuck, A. D.; Raghavachari, K.; Foresman, J. B.; Cioslowski, J.; Ortiz, J. V.; Stefanov, B. B.; Liu, G.; Liashenko, A.; Piskorz, P.; Komaromi, I.; Gomperts, R.; Martin, R. L.; Fox, D. J.; Keith, T.; Al-Laham, M. A.; Peng, C. Y.; Nanayakkara, A.; Gonzalez, C.; Challacombe, M.; Gill, P. M. W.; Johnson, B. G.; Chen, W.; Wong, M. W.; Andres, J. L.; Head-Gordon, M.; Replogle, E. S.; Pople, J. A. *Gaussian 98*, revision A.7; Gaussian, Inc.: Pittsburgh, PA, 1998.

(26) Frisch, M. J.; Pople, J. A.; Binkley, J. S. *J. Chem. Phys*. **1984**, *80*, 3265.

(27) Krishnan, R.; Binkley, J. S.; Seeger, R.; Pople, J. A. *J. Chem. Phys*. **1980**, *72*, 650.

(28) Clark, T.; Chandrasekhar, J.; Spitznagel, G. W.; v. R. Schleyer, P. *J. Comput. Chem*. **1993**, *4*, 294.

(29) Urban, M.; Noga, J.; Cole, S. J.; Bartlett, R. J. *J. Chem. Phys*. **1985**, *83*, 4041.

(30) Bartlett, R. J.; Watts, J. D.; Kucharski, S. A.; Noga, J. *Chem. Phys. Lett*. **1990**, *165*, 513.

(31) Buijse, M. A.; Baerends, E. J. *Density Functional Theory of Molecules, Clusters, and Solids*; Kluwer Academic Publishers: Dordrecht, The Netherlands, 1995.

(32) Scott, A. P.; Radom, L. *J. Phys. Chem*. **1996**, *100*, 16502.

(33) Boys, S. F.; Bernardi, F. *Mol. Phys*. **1970**, *19*, 553.

(34) Lee, T. J. *J. Am. Chem. Soc*. **1989**, *111*, 7362.

(35) Saeki, M.; Tsukuda, T.; Iwata, S.; Nagata, T. *J. Chem. Phys*. **1999**, *111*, 6333.

(36) Novakovskaya, Y. V.; Stepanov, N. F. *Int. J. Quantum Chem*. **1997**, *63*, 737.

(37) Chen, H. Y.; Sheu, W. S. *J. Chem. Phys*. **1999**, *110*, 9032.

(38) Fukui, K. *J. Phys. Chem*. **1970**, *74*, 4161.

(39) Fukui, K. *Acc. Chem. Res*. **1981**, *14*, 363.

(40) Buijse, M. A.; Baerends, E. J. *Theor. Chim. Acta* **1991**, *79*, 389.

(41) Lepetit, M. B.; Malrieu, J. P.; Pelissier, M. *Phys. Rev. A* **1989**, *39*, 981.

(42) Buijse, M. A.; Baerends, E. J. *J. Chem. Phys*. **1990**, *93*, 4129.

(43) Blackman, G. L.; Brown, R. D.; Godfrey, P. D.; Gunn, H. I. *Chem. Phys. Lett*. **1975**, *34*, 241.

(44) Pau, C. F.; Hehre, W. J. *J. Phys. Chem*. **1982**, *86*, 321.

(45) Maki, A. G.; Sams, R. L. *J. Chem. Phys*. **1981**, *75*, 4178.

(46) Brown, R. D. *Nature (London)* **1977**, *270*, 39.

(47) Xantheas, S. S. *J. Chem. Phys*. **1994**, *100*, 7523.

(48) Allamandola, L. J.; Bernstein, M. P.; Sandford, S. A.; Walker, R. L. *Space Sci. Rev*. **1999**, *90*, 219.

(49) d'Hendecourt, L.; Dartois, E. *Spectrochim. Acta* **2001**, *57*, 669.

(50) Goldsmith, P. F.; Ellder, W. D. L. J.; Irvine, W.; Kollberg, E. *Astrophys. J*. **1981**, *249*, 524.

(51) Goldsmith, P. F.; Irvine, W. M.; Hjalmarson, A.; Ellder, J. *Astrophys. J*. **1986**, *310*, 383.

(52) Harwit, M.; Neufeld, D. A.; Melnick, G. J.; Kaufman, M. J. *Astrophys. J*. **1998**, *497*, L105.

(53) Dalby, F. W.; Nielsen, H. H. *J. Chem. Phys*. **1955**, *25*, 934.

(54) Rank, D. H.; Skorinko, G.; Eastman, D. P.; Wiggins, T. A. *J. Mol. Spectrosc*. **1960**, *4*, 518.

(55) Smith, A. M.; Coy, S. L.; Klemperer, W.; Lehmann, K. K. *J. Mol. Spectrosc*. **1989**, *134*, 134.

(56) Winter, M. J.; Jones, W. J. *J. Chem. Soc., Faraday Trans*. **1982**, *78*, 585.

(57) Milligan, D. E.; Jacox, M. E. *J. Chem. Phys.* **1967**, *47*, 278.